DOI: 10.1002/cphc.201000801

Homo-FRET Imaging as a Tool to Quantify Protein and Lipid Clustering**

Arjen N. Bader,[a] Sandra Hoetzl,[b] Erik G. Hofman,[c] Jarno Voortman,[c] Paul M. P. van Bergen en Henegouwen,[c] Gerrit van Meer,[b] and Hans C. Gerritsen*[a]

Homo-FRET, Förster resonance energy transfer between identical fluorophores, can be conveniently measured by observing its effect on the fluorescence anisotropy. This review aims to summarize the possibilities of fluorescence anisotropy imaging techniques to investigate clustering of identical proteins and lipids. Homo-FRET imaging has the ability to determine distances between fluorophores. In addition it can be employed to quantify cluster sizes as well as cluster size distributions. The interpretation of homo-FRET signals is complicated by the fact that both the mutual orientations of the fluorophores and the number of fluorophores per cluster affect the fluorescence anisotropy in a similar way. The properties of the fluorescence probes are very important. Taking these properties into account is critical for the correct interpretation of homo-FRET signals in protein- and lipid-clustering studies. This is be exemplified by studies on the clustering of the lipid raft markers GPI and K-ras, as well as for EGF receptor clustering in the plasma membrane.

1. Introduction

In recent years, Förster resonance energy transfer (FRET)[1] has become a popular tool in biophysics, biochemistry and molecular cell biology.[2–6] FRET is typically used as either a ruler to measure intramolecular distances or to determine molecular colocalization on a nm scale. In the former case, molecules such as proteins are labelled with a suitable (fluorescent) donor and acceptor molecule. The distance between donor and acceptor can be derived from the experimentally determined FRET efficiency.[1]. Changes in the conformational state of the protein, or the cleavage of the protein in two parts can be determined this way.[7] FRET is typically used in protein spectroscopy,[8] molecular sensors[9] and to determine whether two different molecules colocalize on a macromolecular scale, that is, within ~10 nm.[7,10,11] For the latter purpose, FRET can be combined with fluorescence microscopy.[2,3] Molecular organization and protein–protein or protein–ligand interactions in cells can be conveniently visualized in this way.

By far most FRET applications rely on FRET between two different donor and acceptor probes (hetero-FRET), but FRET can also occur between identical fluorophores.[2,12–15] This type of FRET is often referred to as homo-FRET, but the terms homotransfer,[12] donor–donor energy migration[16] or energy migration FRET (emFRET)[17] are also used. In nature, this phenomenon occurs in antenna systems of photosynthetic complexes, for example.[18] As a structural tool in biology, however, it still is not as well established as hetero-FRET. The occurrence of homo-FRET can be observed by its effect on fluorescence anisotropy.[2] This can be implemented in fluorescence microscopes by the addition of polarizing optics. Even 3D confocal anisotropy imaging has been demonstrated.[19] Interestingly, fluorescent labelling is comparatively easy in homo-FRET experiments since only one probe is required. Recent homo-FRET- and fluorescence-anisotropy-related reviews deal with the general concept of fluorescence anisotropy,[20,21] its ability to determine donor–donor distance and mutual orientation,[14] applications to study lipid domains,[22] instrumental aspects,[23] anisotropy imaging of hetero-FRET[24] and anisotropy/homo-FRET in single molecule studies.[25] The current review focuses on application of homo-FRET imaging to quantify the number of fluorophores in small clusters of proteins.

Herein, studies on the plasma membrane organization is used to exemplify the type of information that homo-FRET methods can provide. There has been intensive debate about the heterogeneity of the lipid composition in membranes, that is, the existence of lipid domains (or rafts).[22,26–28] These domains are suggested to play a pivotal role in cellular signalling processes.[29–31] One example shown here concerns the epidermal growth factor receptor (EGFR), an important molecule for the control of cell proliferation.[31,32] This receptor clusters in oligomers after stimulation with its ligand EGF,[33] which stimu-

[a] Dr. A. N. Bader, Prof. Dr. H. C. Gerritsen
Department of Molecular Biophysics
Universiteit Utrecht
Princetonplein 1, 3584 CC Utrecht (The Netherlands)
Fax: (+31) 30 253 2706
E-mail: H.C.Gerritsen@uu.nl

[b] Dr. S. Hoetzl, Prof. Dr. G. van Meer
Department of Membrane Enzymology
Universiteit Utrecht
Padualaan 8, 3584 CH Utrecht (The Netherlands)

[c] Dr. E. G. Hofman, J. Voortman, Dr. P. M. P. van Bergen en Henegouwen
Department of Cellular Dynamics
Universiteit Utrecht
Padualaan 8, 3584 CH Utrecht (The Netherlands)

[**] FRET: Förster Resonance Energy Transfer

Supporting information for this article is available on the WWW under http://dx.doi.org/10.1002/cphc.201000801.

Table 1. Examples of fluorescence depolarization due to homo-FRET.

	Probe	r_{mono}	r_{dimer}	$r_{oligomer}$	r_{dimer}/r_{mono}	$r_{oligomer}/r_{mono}$	Technique	Ref.
Concatamer								
GFP–GFP (dimer) and GFP–GFP–GFP (trimer)	GFP	0.29	0.25	0.21	0.86	0.72	steady state, imaging	[38]
Venus–Venus (dimer) and Venus–Venus–Venus (trimer)	Venus	0.37	0.25	0.18	0.68	0.49	time-resolved, 2PE, spectroscopy	[39]
FKBP–mGFP (dimer) and2×FKBP–mGFP (oligomer)	mGFP	0.38	0.31	0.27	0.82	0.71	time-resolved, imaging	[15]
FKBP–GFP (dimer) and2×FKBP–GFP (oligomer)	GFP	0.38	0.32	0.27[a]	0.84	0.71	time-resolved, imaging	[15]
Protein Oligomers/Aggregrates								
Phospholamban (pentamer)	FlAsH	0.29		0.11		0.38	steady state, spectroscopy	[40]
Herpes simplex virus thymidine kinase (living cells)	GFP	0.25		0.16		0.64	time-resolved, imaging	[13]
Microtubili	FluTax	0.25		0.06		0.24	time-resolved, spectroscopy	[41]
Serotonin-gated 5-HT3 receptor (pentamer)	GFP	0.30		0.22		0.73	steady state	[42]
Ca2+/calmodulin-dependent protein kinase IIα (hexamer)	Venus	0.37		0.12		0.32	time-resolved, 2PE, spectroscopy	[39]
α-Synuclein (in amyloid-like fibrils)	YFP	0.30		0.09		0.30	steady state, imaging	[43]
α-Synuclein (in amyloid-like fibrils)	Alexa488	0.19		0.09		0.47	steady state, imaging	[43]
Lipid-Anchored Proteins in Membranes								
GPI (whole fixed cells)	GFP	0.37		0.25		0.68	time-resolved, spectroscopy	[36]
GPI (living cells)	GFP	0.35		0.32		0.91	time-resolved, spectroscopy	[36]
GPI (living cells)	mYFP	0.34		0.30		0.88	time-resolved, spectroscopy	[36]
GPI (membrane ruffles, fixed cells)	GFP	0.33		0.21		0.64	time-resolved, imaging	[19]
tK (lipid anchor of K-ras)	mGFP	0.38		0.31		0.82	time-resolved, imaging	[a]
Protein Organization in Membranes								
Band 3 protein	Eosin	0.38		0.29		0.76	steady state, spectroscopy	[44]
Epidermal growth factor receptor B1 (living cells)	GFP	0.39		0.34		0.87	steady state, flow cytometry	[17]
EGF receptor (fixed cells)	mGFP	0.38		0.34		0.89	time-resolved, imaging	[32]
EGF receptor (fixed cells, EGF stimulated)	mGFP	0.38		0.28		0.74	time-resolved, imaging	[32]

[a] Unpublished results, see Figure 5 and the Supporting Information.

lates the removal of the activated receptors from the cell surface by receptor mediated endocytosis.[34] Another example is glycosylphosphatidylinositol (GPI) anchored to green fluorescent protein (GFP), a common lipid raft marker that has been one of the key subjects in homo-FRET studies.[15,19,35,36] The last example we present concerns the inner leaflet lipid anchoring of K-ras.[37] Other examples of fluorescence anisotropy based homo-FRET studies are listed in Table 1, which includes information on the observed degree of polarization due to homo-FRET, and the influence of the type of fluorophore on the depolarization.

2. Homo-FRET and Fluorescence Anisotropy

Regular FRET imaging is performed by two-channel ratiometric imaging of donor (I_D) and acceptor (I_A) intensities, spectral imaging, or by fluorescence lifetime imaging.[2] Such approaches do not result in a detectable homo-FRET signal, since in the case of homo-FRET, the donor and acceptor have identical spectroscopic properties. Homo-FRET can be observed, however, by exploiting the difference in polarization of the emission of the fluorophores. Such differences are quantified by the fluorescence anisotropy r [Eq. (1)]:

$$r = \frac{I_{par} - I_{per}}{I_{par} + 2I_{per}} \quad (1)$$

with I_{par} and I_{per} the emission parallel and perpendicular to the excitation polarization direction[1,13,15] (Figure 1).

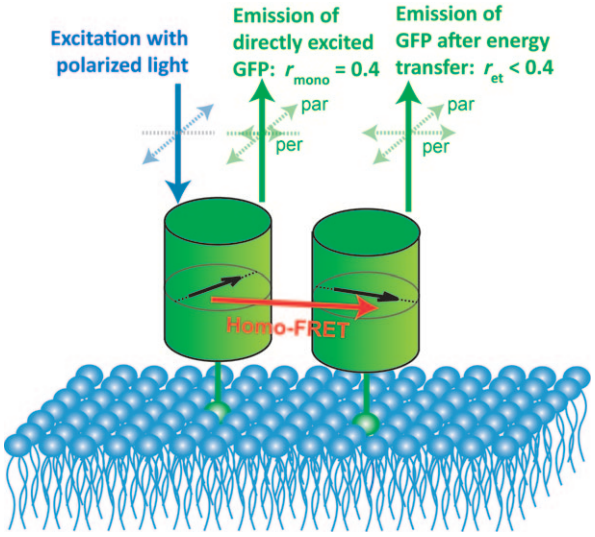

Figure 1. Schematic representation of homo-FRET in a dimer of GFP anchored to a membrane. Adapted from Bader et al.[19]

Excitation with polarized light results in photoselection of fluorophores with their absorption transition dipole moments oriented parallel to the polarization direction of the excitation light. When the emission transition dipole moment is parallel to the absorption transition dipole moment, the anisotropy of this directly excited fluorophore will be maximal. The theoretical value of the maximum amounts to $r = 0.4$ (one-photon excitation).[1] The measured anisotropy is often lower; rotation leads to a broadening of the orientation distribution of the flu-

orophores and consequently a lower anisotropy. When the emission is completely depolarized, $I_{par} = I_{per}$ and the anisotropy is zero. Importantly, energy transfer to neighbouring identical fluorophores will also decrease the anisotropy of the emission. The measured anisotropy is the average of the individual anisotropies of ''directly excited fluorophores'' and ''fluorophores indirectly excited after energy transfer''. The latter fluorophores have not been photoselected by the excitation light, and therefore exhibit a lower anisotropy. The anisotropy reduction depends on the fraction of the emission that originates from these indirectly excited fluorophores (Figure 1).

In microscopy, the use of high numerical aperture objectives results in a reduction of the observed anisotropy.[45] This effect can be corrected for[46] or circumvented by utilizing lower numerical aperture objectives at the price of a loss in resolution and sensitivity. In practice, numerical apertures of 0.7–0.8 are a good compromise.

2.1. The Effect of Homo-FRET and Rotations on Anisotropy

Time-resolved anisotropy measurements offer the possibility to discriminate between anisotropy reduction due to rotation and homo-FRET.[13] Depending on the size of the molecule and the viscosity of the surrounding medium, rotation of molecules can occur on a sub-nanosecond to nanosecond timescale. For a freely rotating (spherical) molecule in solution in the absence of homo-FRET, this decay is described by Equation (2):

$$r(t) = r_0 e^{-t/\Phi} \quad (2)$$

where Φ is the rotation correlation time of the rotor and r_0 is the maximum initial anisotropy.[1] r_0 is determined by the angle between the excitation and the emission dipole moments. For a fluorophore in solution, $r(t)$ goes to zero for time infinity.

In the case of homo-FRET, the time dependency of the anisotropy depends on the rate of energy transfer. In the absence of rotation, the time-resolved anisotropy decay due to homo-FRET can be written as Equation (3):[13,47]

$$r(t) = (r_0 - r_{inf})e^{-2\omega t} + r_{inf} \quad (3)$$

Here, ω denotes the homo energy transfer rate [Eq. (4)]:

$$\omega = \left(R_0/R\right)^6 \tau^{-1} \quad (4)$$

where R_0 is the Förster distance, R the interfluorophore distance and τ the fluorescence lifetime in the absence of FRET. ω is related to the energy transfer efficiency E by Equation (5):

$$E = \omega/(\tau^{-1} + \omega) \quad (5)$$

The total reduction in anisotropy due to homo-FRET depends on the number of fluorophores per cluster and their relative orientation (see Sections 2.2 and 2.3). Importantly, when the number of fluorophores in the cluster increases, a larger fraction of the fluorescence will originate from indirectly (by energy transfer) excited fluorophores with comparatively low anisotropy. The anisotropy after energy transfer is determined by the orientation of the indirectly excited fluorophores with respect to the orientation of the directly excited fluorophore. With increasing mutual orientations, the anisotropy after energy transfer becomes lower.

To separate homo-FRET from rotational depolarization, it is advantageous to employ slowly rotating dye molecules such as fluorescent proteins (rotational correlation time $\Phi \gg \tau$). Intrasequence expression of GFP can further reduce rotations.[48] Now, rotations can be ignored and the analysis of the anisotropy decay is comparatively simple. For small fluorophores (organic dyes), the molecular rotations are typically fast. However, because the fluorophores are usually covalently bound to large proteins, rotation is hindered along one or two of the possible rotation axes. Consequently, the anisotropy decay becomes multiexponential.[1] Reliable analysis of such multiexponential decays requires high signal levels and can be complicated.

2.2. Orientation of Fluorophores

For homo-FRET in dimers, the mutual orientation of the fluorophores can be determined. According to Tanaka et al.[47] and Gautier et al.,[13] the dependence of $r(t)$ on the mutual orientation of the transition dipole moments Θ of two fluorophores in a dimer is given by Equation (6):

$$r(t) = 0.1[(3 - 3\cos^2\theta)e^{-2\omega t} + 3\cos^2\theta + 1] \quad (6)$$

This equation is only valid for fluorophores with parallel absorption and emission transition dipole moments. For randomly oriented molecules, the anisotropy after one energy transfer step is 0.016.[12,49] For $t \rightarrow \infty$, energy transfer between the two fluorophores occurs many times and there is a 50% chance that the directly excited fluorophores emits a photon (with $r \approx 0.4$), and a 50% chance that the indirectly excited fluorophores emits a photon (with $r \approx 0$); the average dimer anisotropy at $r(\infty)$ will therefore be ~0.2. According to equation 6, this corresponds to an average mutual orientation between the fluorophores of ~54°.

In practice, the molecules in a dimer or oligomer are often not randomly oriented. This has been verified in experiments involving controlled dimerisation and oligomerization of fluorescent proteins.[15,38,39] For instance, controlled dimerization of mGFP (monomeric GFP) using the protein dimerization construct FKBP (FK506 binding protein) leads to a decrease in the time-resolved anisotropy from 0.38 to 0.30 (Table 1).[15] This is much less than expected from randomly oriented molecules and, according to Equation (6), this corresponds to an average Θ for the mGFP dimer of ~30°. In these experiments, the anisotropy reduction was shown to be independent of the inclusion of a flexible linker and the exchange of mGFP for GFP.[15] These results suggest that the mutual orientation is an intrinsic property of the fluorescent proteins themselves. Preferred relative orientations of the GFPs are a likely explanation for the

comparatively low anisotropy reductions found in many experiments.[15]

When GFP is mutated into for instance YFP (yellow fluorescent protein), or Venus, the mutual orientation may be altered due to 1) a rotation of the absorption/emission transition dipole moment of the fluorophore, 2) a different orientation of the fluorophore in the barrel, and 3) chemical interactions between the barrels. This difference in mutual orientation might explain the difference in depolarization found for GFP–GFP[38] and Venus–Venus dimeric concatamers,[39] as well as for GPI–GFP and GPI–mYFP in cell membranes[36] (Table 1). However, no comparative study on the mutual orientation of fluorescent protein dimers has been carried out yet. We note that the effects of preferred orientations may have a strong effect on the quantification of the number of fluorophores per cluster (Section 2.3).

2.3. Number of Fluorophores per Cluster

An important application of homo-FRET imaging is the determination of the number of fluorophores per cluster. According to the theory proposed by Runnels and Scarlata,[12] the fluorophores in homo-FRET clusters are divided in two pools: directly excited fluorophores and indirectly excited fluorophores. Considering a cluster of N fluorophores, only one fluorophore is directly excited (fraction $1/N$, high anisotropy r_{mono}) while the remaining fluorophores are indirectly excited (fraction $(N-1)/N$, lower average anisotropy r_{et}). When the efficiency of the transfer is low, the majority of the emission originates from directly excited fluorophores. Conversely, a higher energy transfer rate increases the probability that the indirectly excited fluorophores emit. Averaged over a large number of clusters of on average N fluorophores, the bulk steady-state anisotropy (in the absence of rotation) is therefore given by Equation (7):

$$r_N = r_{mono}\frac{1+\omega\tau}{1+N\omega\tau} + r_{et}\frac{(N-1)\omega\tau}{1+N\omega\tau} \quad (7)$$

The factor $\omega\tau$ is included to correct for the effect of energy transfer efficiency. Although this theory is useful in direct quantification of protein clustering, it should be handled with care. The major disadvantage of the theory is that it assumes a constant average anisotropy for all the indirectly excited fluorophores (i.e. r_{et}), even after multiple energy transfer steps. This is true when the mutual orientation of the fluorophores is random and r_{et} thus approximates zero. In other cases, a more extensive relation between anisotropy and cluster size should be derived.

For most fluorescent proteins, the anisotropy decrease due to homo-FRET is only small. For a reference construct containing two GFPs, the anisotropy is typically reduced by 20–30% (see Table 1).[15,38,39] This minor anisotropy decrease was attributed to orientation effects.[15,38] For pentameric Phospholamban-FlAsH, on the other hand, the anisotropy is reduced by 62%. In the latter case, the deviation from Runnels and Scarlata theory was attributed to the sub-stoichiometrical labelling rather than orientation effects.[40] These examples demonstrate that the choice of probe is important in homo-FRET cluster size determination.

The anisotropies of oligomers found in various homo-FRET studies are compared in Table 1. Anisotropy reductions of more than 50% are observed for protein fibres like microtubili[41] and amyloid-like fibrils.[43] According to Runnels and Scarlata theory, this means that the fluorophores are oligomerized. In membranes, however, the largest anisotropy reduction listed here is only 36%, which suggests that the average size of lipid or protein receptor clusters is small.

3. Quantifying Cellular Membrane Organization

Regular FRET imaging is a common tool to investigate membrane organization.[22,50,51] It has been utilized for example, to determine the colocalization of lipid probes[52] as well as the colocalization between proteins and (protein-bound) lipids.[31,53] Alternatively, fluorescence anisotropy experiments have been performed to determine the lipid order of membranes.[54,55]

3.1. Verification of the Occurrence of Homo-FRET

A typical example of a homo-FRET study is the determination of the distribution of membrane-anchored proteins in the plasma membrane. Here, GFP linked to a glycosylphosphatidylinositol (GPI) anchor is often used. GPI-anchored proteins are transferred via the Golgi apparatus to the plasma membrane where they are found in nanoscale clusters.[35,36] GPI–GFP expressed in NIH 3T3 cells clearly shows its presence in both the Golgi and the plasma membrane (Figure 2A). A large difference in anisotropy is found between GPI–GFP in the interior of the cell and GPI–GFP in the plasma membrane.[19] To ensure that the reduced anisotropy of GPI–GFP is due to homo-FRET, multiple tests can be performed. The best proof that homo-FRET occurs can be obtained from time-resolved anisotropy decays.[13–16,19,22,36,39,41] The reference anisotropy decay of a monomeric GFP (mGFP) in solution typically exhibits a slow decay due to the slow rotation of the relatively large GFP (~28 kDa); the anisotropy is high and virtually constant (Figure 2B, left). Homo-FRET results in a rapid depolarization that levels off [Eq. (3)], confirming the occurrence of homo-FRET in clusters of GPI–GFPs in the plasma membrane. As a control experiment the GPI clusters can be disrupted by removal of cholesterol form the plasma membrane. Cholesterol can be depleted by treatment with saponin which indeed results in disappearance of homo-FRET.[36]

Alternative approaches to verify the occurrence of homo-FRET are red edge excitation and fractional labelling. The former takes advantage of Weber's red edge effect, that is, the vanishing of homo-FRET when exciting fluorophores at the red edge of the absorption spectrum.[56] Nowadays, it is used to confirm the existence of homo-FRET in spectroscopy[44] and imaging.[38] A second approach is to fractionally label the target or photobleach part of the fluorophores.[17,35,36,44,57,58] This reduction of the number of fluorophores will decrease the

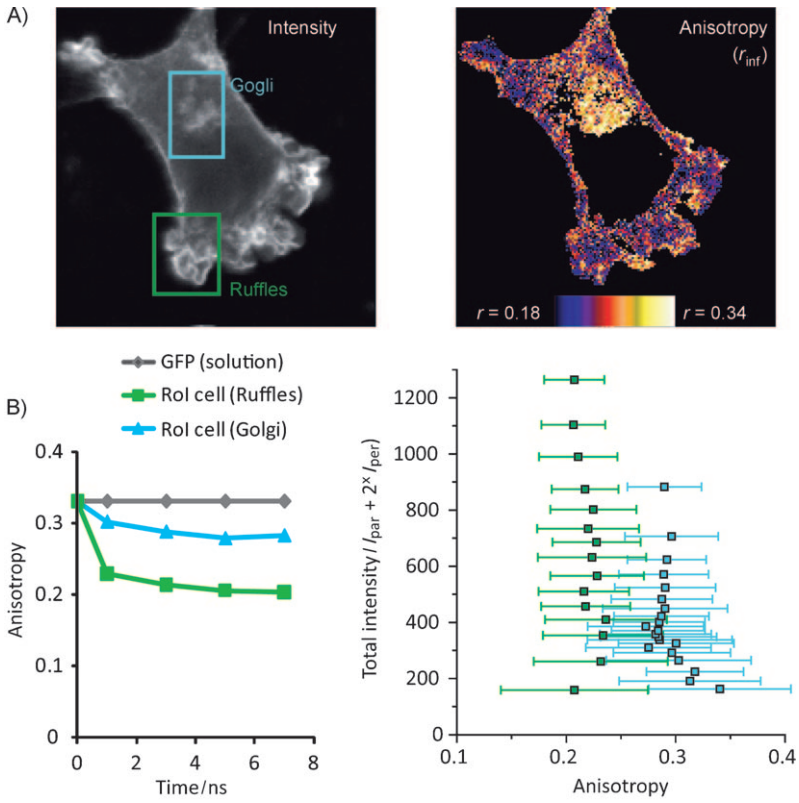

Figure 2. A) Intensity and anisotropy (r_{inf}) image of a Her14 cell expressing GPI–GFP. B) Homo-FRET analysis of two regions of interest indicated in the intensity image (blue = Golgi; green = membrane ruffles). Left: time-resolved anisotropy decays, right: anisotropy plotted versus the intensity for each pixel. Adapted from Bader et al.[19]

measured homo-FRET; a higher anisotropy in fractionally labelled or photobleached samples therefore confirms the occurrence of homo-FRET.

3.2. Nanoscale Organization or Concentration Clustering?

Potentially, homo-FRET can be induced by nanoscale biochemical interactions or high dye concentrations due to overexpression. This is particularly important when homo-FRET is studied in membranes; concentration FRET in a '2D plane' is much more likely than in a 3D solution. Nanometer-scale organization can be conveniently discriminated from a random distribution (i.e. concentration clustering) by analysing scatter plots of the intensity (fluorophore concentration) and the corresponding anisotropy (degree of homo-FRET) values of the pixels in an image.[35] For the GPI–GFP experiments, there is no correlation between intensity and anisotropy (Figure 2B, right). A higher fluorophore density does not result in increased clustering, suggesting that the observed clustering is induced by non-random biochemical interactions between GPI–GFP in domains.[19,35] This provides evidence for the nanoscale organization of GPI-anchored proteins in plasma membrane domains.[35]

3.3. Direct Quantification of Protein Cluster Sizes

Runnels and Scarlata theory can also be used to determine the average number of proteins in a cluster. However, as explained above, the measured anisotropy does not only depend on the number of proteins in a cluster, but also on the energy transfer efficiency [$\omega\tau = E/(E-1)$] and the mutual orientation of the fluorophores (r_{et}). Moreover, the labelling stoichiometry also affects the measured cluster size. This is especially important for labelling with organic dyes, but incomplete maturation of fluorescent proteins can reduce the labelling stoichiometry as well. For GFP, typically 80% of the expressed protein actually fluoresces whereas the remainder is immature.[59]

The effect of the energy transfer efficiency is taken into account by utilizing time-resolved anisotropy detection. Note that in time-resolved experiments, the anisotropy decreases to a level (r_{inf}) where energy transfer has occurred multiple times and all fluorophores in the cluster have equal probability of emitting a photon. Since r_{inf} does not depend on the transfer efficiency, it can act as a more accurate measure of clustering.[19]

The mutual orientation of the fluorophores determines to which extent the anisotropy is reduced by the energy transfer [in Eq. (7) this is included in r_{et}]. In recent experiments, it was suggested that the mutual orientation of GFPs is mainly determined by the fluorophore itself.[15] When the homo-FRET efficiency is high, as can be inferred from the time-resolved anisotropy decay, the distance between the fluorophores is short (note that the Förster distance for GFP homo-FRET is 4.65 nm).[36] For GFP, the distance is often comparable with the dimensions of its barrel (~2 by ~4 nm).[60] On this length scale, weak chemical interaction between the barrels of (m)GFPs can easily occur. Interestingly, short-range interactions are often independent of the remaining part of the GFP construct.[15] Therefore, reference anisotropy measurements can be performed on model GFP constructs to calibrate the (limiting) anisotropy of monomers, dimers, and so forth. For example, the protein subunit FKBP can be dimerized by the binding of the ligand AP20187. A FKBP–mGFP construct is used to calibrate the anisotropy of mGFP dimers, and a construct with two FKBP domains (2×FKBP–mGFP) to calibrate the anisotropy of oligomers (Figures 3A,B).[15] Other reference constructs employed include FKBP fused to GFP, FKBP fused to mGFP via a flexible linker and a construct where FKBP–mGFP are fused to the transmembrane protein EGF receptor (EGFR).[15,32] In all cases the anisotropy reduction after induced clustering was approximately the same: ~20% reduction after dimerization and

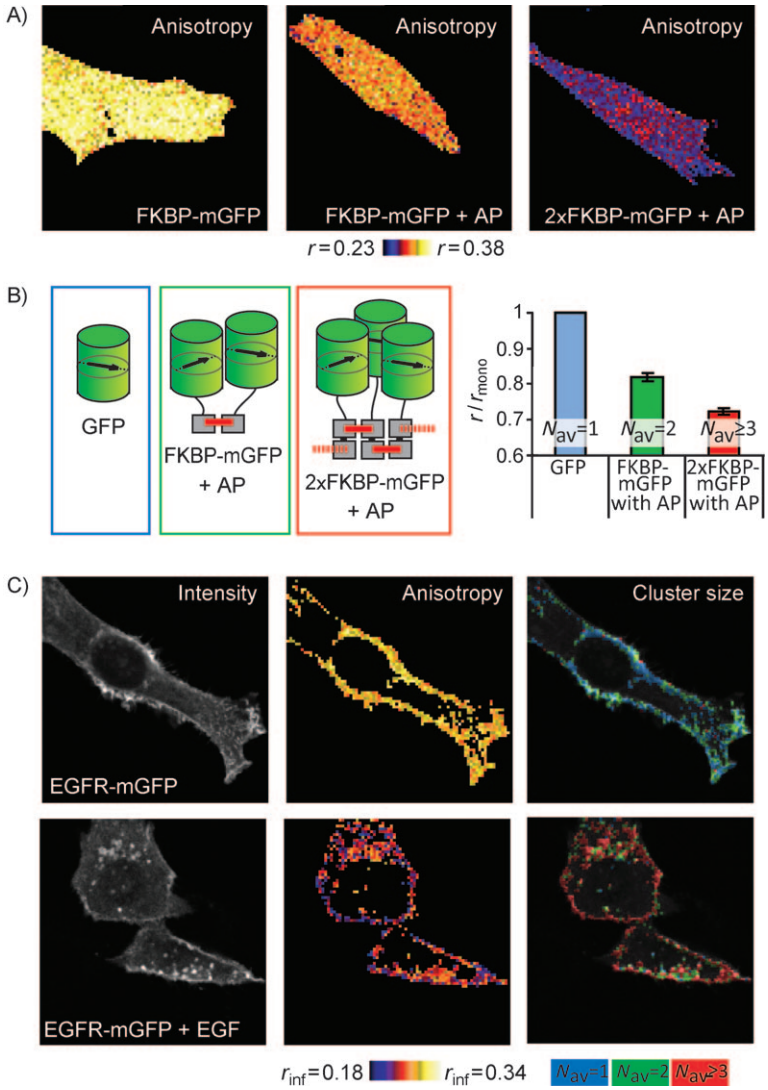

Figure 3. A) Anisotropy images of cells expressing the constructs FKBP–mGFP (monomers), FKBP–mGFP (incubated with ligand AP20187 to form dimers), and 2×FKBP–mGFP (incubated with ligand AP20187 to form oligomers). B) The constructs and the ligand (when added), and the average anisotropy reduction in the images in (A). C) Intensity, anisotropy and cluster-size image of cell expressing EGFR–GFP (in resting cells and 5 min after stimulation with EGF). In the latter image, the anisotropy values are categorized in $N_{av}=1$, $N_{av}=2$ and $N_{av}\geq 3$, based on the calibration performed in (B). Adapted from Bader et al.[15] and Hofman et al.[32] A more detailed description can be found in these references.

~30% reduction after oligomerization (Figures 3A,B).[15,32] In the case of GFP, the anisotropy values in an image can therefore be divided in three categories: $N_{av}=1$ (i.e. on average monomers), $N_{av}=2$ (i.e. on average dimers) and $N_{av}\geq 3$ (i.e. on average oligomers). In this way, clustering maps of proteins in cells can be constructed. The resolvability of cluster sizes is limited by photon statistics.[61] Typically 1000 counts per pixel are needed for discrimination of $N_{av}=1,2,>3$. In summary, calibration with reference constructs circumvents the issue of nonrandom mutual orientations of the fluorescent probes. Moreover, underestimation of the cluster size because of incomplete maturation of the fluorescent protein is no longer an issue. The validity of utilizing reference construct should always be checked, for example by verifying that the distance between the fluorophores is less than ~4 nm (meaning that there are weak chemical interactions between fluorescent protein barrels).

The application of cluster-size imaging to study the clustering of EGF receptors is demonstrated in Figure 3C.[32] In resting cells, EGFR-mGFP is mainly localized in the plasma membrane. The cluster-size image shows that EGFR–mGFP is already partly clustered in predimers/pre-oligomers. After activation with EGF, the receptors are internalized (intensity image Figure 3C) in endosomes.[32] Both in the plasma membrane and in endosomes, EGFR is now oligomerized (cluster-size image Figure 3C).

3.4. Distribution of Protein Clusters

By applying fractional labelling or partial photobleaching, additional information can be obtained in homo-FRET studies (Section 3.1). The plot of the anisotropy as a function of the fraction of labelled target can reveal the distribution of cluster sizes. Bleaching or fractional labelling of monomers does not change the anisotropy. For dimers the plot will be a straight line. Higher-order clusters result in increased curvature of the plot. When two distributions of cluster sizes with the same anisotropy (for example 100% dimers and 50% monomer + 50% trimers) are compared, the fractional labelling behaviour will be different. This concept was introduced by Sharma et al.[36] (partial photobleaching), and Yeow and Clayton[58] (fractional labelling). In both cases, a polynomial of the order $N-1$, (N being the number of fluorophores per cluster) describes the anisotropy dependence on partial photobleaching/fractional labelling. N can be found by comparing experimental data with the calculated fractional labelling dependence of the anisotropy of model cluster size distributions. Partial photobleaching has the advantage that it can be performed on the same sample, but artifacts might be introduced when the photobleaching products affect the fluorescent properties of the remaining probes. Conversely, fractional labelling is difficult to perform with fluorescent protein, since it might be difficult to accurately verify what the fraction of labelled and unlabeled target protein is.

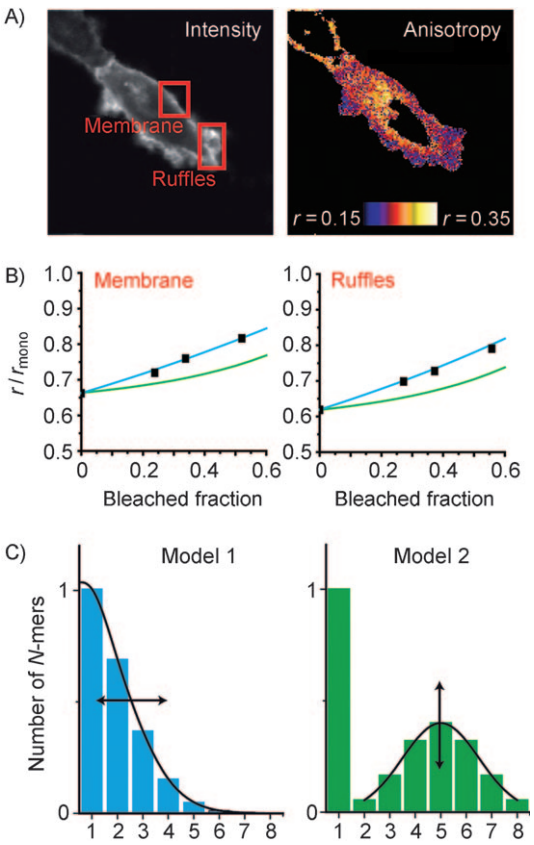

Figure 4. A) Intensity and anisotropy image of cells expressing GPI-GFP. B) Controlled photobleaching increases the relative anisotropy (r/r_{mono}, black spots) in two regions of interest (indicated in A). C) Two models for cluster-size distributions. Calculated anisotropies after controlled photobleaching of these model distributions (model 1: blue, model 2: green) are depicted in (B). Adapted from Bader et al.[19]

As an example, controlled photobleaching results are shown in Figure 4B of a cell expressing GPI–GFP.[19] In this case, the relative anisotropy (r/r_{mono}) is plotted vs the bleached fraction (I/I_{mono}) for two different regions, plasma membrane and membrane ruffles. The data were compared to data obtained from simulations of two protein cluster models: a distribution of small clusters (model 1, see Figure 4C) and a distribution of large clusters + monomers (model 2). The data compares best with model 1 for both regions in the cell, confirming the work of Sharma et al.[36] For the EGF receptor, an anisotropy study utilizing fractional labelling also suggests mainly small clusters.[58]

4. Interpretation of Homo-FRET Clusters

The overview of homo-FRET studies on different proteins that is presented in Table 1 shows that in most homo-FRET studies only minor depolarization was found (for membrane protein up to 36% reduction of r), which suggests that the clusters are typically small. This raises the question whether large clusters were not present in these studies or that large-scale clustering cannot be determined using homo-FRET. Typical dimensions of GFP are ~4 nm, which is comparable to the homo-FRET Förster distances of ~4.6.[36] Transmembrane receptors are often larger; for example, the EGF receptor covers a >5 nm diameter area in the plasma membrane. So, when the EGF receptor or GPI-GFP is clustered, there will only be a few fluorophores within the Förster distance. Only when the distance between the donors is short (high fluorophore density), the efficiency of homo-FRET is sufficient to observe larger clusters. It is important to realize that the absence of a homo-FRET signal does not necessarily exclude the existence of clustering on a scale larger than the Förster distance (i.e. more than ~10 nm). Other techniques like electron microscopy, near-field optical scanning microscopy and single-particle tracking show that lipid domains can be larger.[62–64] Typically, these domains are smaller than the resolution of an optical microscope (200 nm), but they are larger than the length scale over which FRET can occur.

To detect larger cluster sizes, electron microscopy in combination with immunogold labeling can be applied. An example of such an approach concerns the analysis of the inner leaflet raft marker tK–mGFP (K-ras analogue) using both homo-FRET and electron microscopy (EM) (see the Supporting Information for details). Cells expressing tK–mGFP were split using freeze-fraction, resulting in isolated plasma membrane sheets on a surface. The membrane sheets were fixed and immunolabeled using gold particles (10 nm) conjugated to rabbit anti-GFP. The distribution of the gold particles on plasma membrane sheets was analysed using Ripley's K-function[63] (Figure 5A). Domains of on average five tK–mGFP molecules within a radius of approximately 25 nm were observed. Homo-FRET analysis, analogous to experiments shown in the Figures 2, 3, shows that concentration-independent homo-FRET occurs in clusters of on average two tK–mGFP molecules. Note that this analysis was done on the same constructs that were expressed in the same cell type.

The difference in the observed degree of clustering is an inherent consequence of the limitations of the techniques that are used. Homo-FRET can only discriminate clustering on a molecular scale (up to 5–10 nm) and the immuno-EM analysis is restricted by the size of the gold labelling. The latter depends both on the size of the antibody (~10 nm) and the size of the immuno-gold particle, which results in a minimum domain size of ~10 nm. The two techniques are therefore complementary; using homo-FRET only domains smaller than ~10 nm and using EM only domains larger than ~10 nm can be distinguished. Homo-FRET analysis of the tK–GFP distribution reveals the presence of 5 nm clusters of predominantly dimers (Figure 5B). EM analysis reveals the presence of a larger number of tK–GFPs in domains of ~25 nm (Figure 6A). Using these complementary results, a model is made to describe the distribution of tK–mGFP in the inner leaflet of the plasma membrane (Figure 6). Small molecular-scale clusters that are present in larger-scale domains (~25 nm) (Model D, Figure 6). An interesting question is whether the homo-FRET clustering within these domains is induced by 1) the interaction between the lipid anchors, or 2) by interactions between GFP barrels. Indeed, it has been shown that tK(ras) partitions in domains that consist of typical raft lipids as sphingolipids and cholesterol. Moreover,

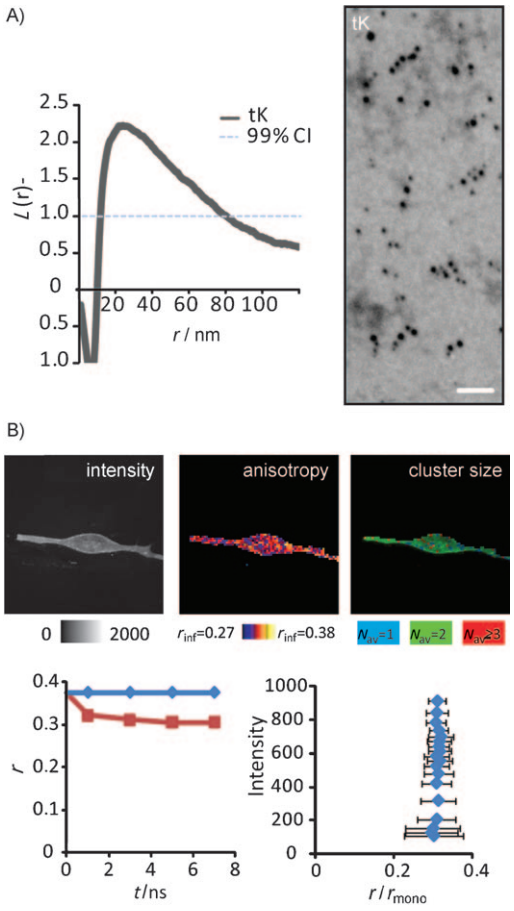

Figure 5. Comparison of immuno-EM and homo-FRET analysis of the clustering of inner leaflet raft marker tK in the cellular plasma membrane of GM95 cells. A) immuno-EM image of tK labelled with gold particles and analysis with Ripley's K-function on the size of the clusters. Bar is 50 nm. B) Homo-FRET images of cell expressing tK–mGFP (intensity, anisotropy and cluster size), time-resolved anisotropy decays (averaged over the whole image in red and for GFP in solution in blue) and scatter plot of intensity versus anisotropy. Data analysed analogous to Figure 2 and Figure 3. See the Supporting Information for details.

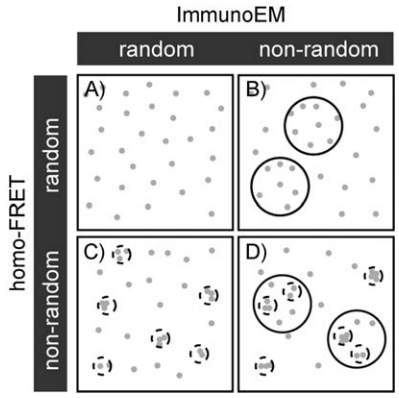

Figure 6. Complementary scales of clustering observed by immunoEM and homo-FRET.

there are weak chemical interactions between mGFP barrels in clusters. Partitioning of tK–GFP in lipid domains might result in higher local concentration of the probe, and multiple low k_D interactions between either the anchor or the GFP might induce a process indicated as avidity in protein clustering. In all cases, homo-FRET will occur. Homo-FRET is not dependent upon the concentration of tK–GFP in the plasma membrane (Figure 5 B), indicating that nanoscale organization of tK–GFP is most likely the result of the partitioning in lipid domain structures or lipid rafts.

5. Summary and Outlook

Homo-FRET imaging is a powerful tool to study protein and lipid clustering on a nanometer scale. This technique reveals information on the number of fluorophores per cluster and the distribution of cluster sizes. The presence of a homo-FRET signal is indicative of interactions on a molecular level. However, the maximum cluster size that can be observed is limited, as homo-FRET is not sensitive to large-scale organization. Computer simulations on homo-FRET clusters in membranes can provide a better insight in the range over which homo-FRET can occur and improve our understanding of the relation between cluster size and anisotropy decrease.

In homo-FRET imaging, the choice of the probe is more critical than in regular FRET studies. Depolarization due to rotations can be separated from homo-FRET by employing fluorescent proteins. Organic dyes frequently exhibit rapid rotations, which complicate the homo-FRET analysis. The use of fluorescent proteins may complicate homo-FRET by preferred orientations of these proteins. The mutual orientation of the probes is determined by the orientation of the transition dipole moment in the barrel, as well as the possible interactions between the barrels. When organic dyes are employed, the labelling stoichiometry is critical and often unknown. Homo-FRET imaging would benefit from extensive comparative studies of fluorophores, including studies involving controlled dimerization. Ideally, optimized homo-FRET probes exhibit large drops in anisotropy after energy transfer.

It should be stressed that homo-FRET based techniques only provide information on a length scale comparable to the Förster radius (5–10 nm). The observation that homo-FRET clusters exist does not exclude the possibility of larger-scale organization. Inversely, within large-scale domains (tens or hundreds of nanometers in diameter), there can be subdomain organization as well. Therefore, in an ideal case cluster size studies combine homo-FRET with complementary high-resolution (imaging) techniques such as electron microscopy,[65] correlation spectroscopy,[66] far-field optical nanoscopy[67] and others.[51] Such measurements will be valuable for clarifying conflicting results obtained with different techniques (for example about the fraction of EGFR predimers in the plasma membrane.[15,68–70] Finally, homo-FRET analysis can easily be integrated in conventional fluorescence microscopes. The only requirement being that the instrument is equipped with a set of polarizers, and that sufficient signal is accumulated. This method has the potential to provide important insights in the organization of cells and cell membranes.

Acknowledgements

This research was supported in part by the Dutch Organization for Scientific Research [NWO-ALW, Molecule to Cell (MtC) program] (A.N.B., S.H. and E.G.H.).

Keywords: fluorescence anisotropy · fluorescence microscopy · FRET · lipids · proteins

[1] B. Valeur, *Molecular Fluorescence. Principles and Applications*, Wiley-VCH, Weinheim, **2002**.
[2] E. A. Jares-Erijman, T. M. Jovin, *Nat. Biotechnol.* **2003**, *21*, 1387 – 1395.
[3] G. W. Gordon, G. Berry, X. H. Liang, B. Levine, B. Herman, *Biophys. J.* **1998**, *74*, 2702 – 2713.
[4] R. M. Clegg, *Laboratory Techniques in Biochemistry and Molecular Biology, Vol. 33*, (Ed.: T. W. J. Gadella) **2009**, Chap. 1, pp 1–57.
[5] V. E. Centonze, M. Sun, A. Masuda, H. Gerritsen, B. Herman, *Methods Enzymol.* **2003**, *360*, 542 – 560.
[6] R. M. Clegg, *Curr. Opin. Biotechnol.* **1995**, *6*, 103 – 110.
[7] K. Truong, M. Ikura, *Curr. Opin. Struct. Biol.* **2001**, *11*, 573 – 578.
[8] T. Ha, *Methods* **2001**, *25*, 78 – 86.
[9] B. Ananthanarayanan, Q. Ni, J. Zhang, *Methods Cell Biol.* **2008**, *89*, 37 – 57.
[10] A. Periasamy, H. Wallrabe, Y. Chen, M. Barroso, *Methods Cell Biol.* **2008**, *89*, 569 – 598.
[11] Y. Chen, J. D. Mills, A. Periasamy, *Differentiation* **2003**, *71*, 528 – 541.
[12] L. W. Runnels, S. F. Scarlata, *Biophys. J.* **1995**, *69*, 1569 – 1583.
[13] I. Gautier, M. Tramier, C. Durieux, J. Coppey, R. B. Pansu, J. C. Nicolas, K. Kemnitz, M. Coppey-Moisan, *Biophys. J.* **2001**, *80*, 3000 – 3008.
[14] M. Tramier, M. Coppey-Moisan, *Methods Cell Biol.* **2008**, *85*, 395 – 414.
[15] A. N. Bader, E. G. Hofman, J. Voortman, P. M. P. Van Bergen En Henegouwen, H. C. Gerritsen, *Biophys. J.* **2009**, *97*, 2613 – 2622.
[16] S. Kalinin, L. B. Johansson, *J. Fluoresc.* **2004**, *14*, 681 – 691.
[17] D. S. Lidke, P. Nagy, B. G. Barisas, R. Heintzmann, J. N. Post, K. A. Lidke, A. H. A. Clayton, D. J. Arndt-Jovin, T. M. Jovin, *Biochem. Soc. Trans.* **2003**, *31*, 1020 – 1027.
[18] S. Akimoto, M. Mimuro, *Photochem. Photobiol.* **2007**, *83*, 163 – 170.
[19] A. N. Bader, E. G. Hofman, P. M. P. Van Bergen en Henegouwen, H. C. Gerritsen, *Opt. Express* **2007**, *15*, 6934 – 6945.
[20] D. M. Jameson, J. A. Ross, *Chem. Rev.* **2010**, *110*, 2685 – 2708.
[21] S. S. Vogel, C. Thaler, P. S. Blank, S. V. Koushik in *FLIM Microscopy in Biology and Medicine* (Eds.: A. Periasamy, R. M. Clegg), CRC Press, Boca Raton, **2009**, 245 – 290.
[22] M. Rao, S. Mayor, *Biochim. Biophys. Acta Mol. Cell Res.* **2005**, *1746*, 221 – 233.
[23] J. A. Levitt, D. R. Matthews, S. M. Ameer-Beg, K. Suhling, *Curr. Opin. Biotechnol.* **2009**, *20*, 28 – 36.
[24] D. W. Piston, M. A. Rizzo, *Methods Cell Biol.* **2008**, *85*, 415 – 430.
[25] C. C. Gradinaru, D. O. Marushchak, M. Samim, U. J. Krull, *Analyst* **2010**, *135*, 452 – 459.
[26] K. Simons, G. Van Meer, *Biochemistry* **1988**, *27*, 6197 – 6202.
[27] M. Edidin, *Annu. Rev. Biophys. Biomol. Struct.* **2003**, *32*, 257 – 283.
[28] D. Lingwood, K. Simons, *Science* **2010**, *327*, 46 – 50.
[29] D. A. Brown, E. London, *Annu. Rev. Cell Dev. Biol.* **1998**, *14*, 111 – 136.
[30] G. Van Meer, D. R. Voelker, G. W. Feigenson, *Nat. Rev. Mol. Cell Biol.* **2008**, *9*, 112 – 124.
[31] E. G. Hofman, M. O. Ruonala, A. N. Bader, D. van den Heuvel, J. Voortman, R. C. Roovers, A. J. Verkleij, H. C. Gerritsen, P. M. P. van Bergen en Henegouwen, *J. Cell Sci.* **2008**, *121*, 2519 – 2528.
[32] E. G. Hofman, A. N. Bader, J. Voortman, D. J. Van den Heuvel, S. Sigismund, A. J. Verkleij, H. C. Gerritsen, P. M. P. van Bergen en Henegouwen, *J. Chem. Biol.*, DOI: 10.1074/jbc.M110.164731.
[33] P. J. Verveer, F. S. Wouters, A. R. Reynolds, P. I. H. Bastiaens, *Science* **2000**, *290*, 1567 – 1570.
[34] S. Sigismund, T. Woelk, C. Puri, E. Maspero, C. Tacchetti, P. Transidico, P. P. Di Fiore, S. Polo, *Proc. Natl. Acad. Sci. USA* **2005**, *102*, 2760 – 2765.
[35] R. Varma, S. Mayor, *Nature* **1998**, *394*, 798 – 801.
[36] P. Sharma, R. Varma, R. C. Sarasij, Ira, K. Gousset, G. Krishnamoorthy, M. Rao, S. Mayor, *Cell* **2004**, *116*, 577 – 589.
[37] D. Abankwa, A. A. Gorfe, J. F. Hancock, *Semin. Cell Dev. Biol.* **2007**, *18*, 599 – 607.
[38] A. Squire, P. J. Verveer, O. Rocks, P. I. H. Bastiaens, *J. Struct. Biol.* **2004**, *147*, 62 – 69.
[39] C. Thaler, S. V. Koushik, H. L. Puhl III, P. S. Blank, S. S. Vogel, *Proc. Natl. Acad. Sci. USA* **2009**, *106*, 6369 – 6374.
[40] S. L. Robia, N. C. Flohr, D. D. Thomas, *Biochemistry* **2005**, *44*, 4302 – 4311.
[41] M. P. Lillo, O. Canadas, R. E. Dale, A. U. Acuna, *Biochemistry* **2002**, *41*, 12436 – 12449.
[42] E. Ilegems, H. Pick, C. Deluz, S. Kellenberger, H. Vogel, *ChemBioChem* **2005**, *6*, 2180 – 2185.
[43] T. J. van Ham, A. Esposito, J. R. Kumita, S. T. D. Hsu, G. S. Kaminski Schierle, C. F. Kaminski, C. M. Dobson, E. A. A. Nollen, C. W. Bertoncini, *J. Mol. Biol.* **2010**, *395*, 627 – 642.
[44] S. M. Blackman, D. W. Piston, A. H. Beth, *Biophys. J.* **1998**, *75*, 1117 – 1130.
[45] D. Axelrod, *Biophys. J.* **1979**, *26*, 557 – 573.
[46] J. J. Fisz, *J. Phys. Chem. A* **2007**, *111*, 8606 – 8621.
[47] F. Tanaka, N. Mataga, *Photochem. Photobiol.* **1979**, *29*, 1091 – 1097.
[48] J. V. Rocheleau, M. Edidin, D. W. Piston, *Biophys. J.* **2003**, *84*, 4078 – 4086.
[49] V. M. Arganovich, M. D. Galanin, *Electronic Excitation Energy Transfer in Condensed Matter*, North-Holland Publishing, Amsterdam, **1982**.
[50] D. M. Owen, D. Williamson, C. Rentero, K. Gaus, *Traffic* **2009**, *10*, 962 – 971.
[51] B. C. Lagerholm, G. E. Weinreb, K. Jacobson, N. L. Thompson, *Annu. Rev. Phys. Chem.* **2005**, *56*, 309 – 336.
[52] P. Sengupta, D. Holowka, B. Baird, *Biophys. J.* **2007**, *92*, 3564 – 3574.
[53] A. K. Kenworthy, N. Petranova, M. Edidin, *Mol. Biol. Cell* **2000**, *11*, 1645 – 1655.
[54] A. Gasecka, T. Han, C. Favard, B. R. Cho, S. Brasselet, *Biophys. J.* **2009**, *97*, 2854 – 2862.
[55] A. Gidwani, D. Holowka, B. Baird, *Biochemistry* **2001**, *40*, 12422 – 12429.
[56] G. Weber, *Biochem. J.* **1960**, *75*, 335 – 345.
[57] L. Bene, J. Szollosi, G. Szentesi, L. Damjanovich, R. Gaspar, T. A. Waldmann, S. Damjanovich, *Biochim. Biophys. Acta Mol. Cell Res.* **2005**, *1744*, 176 – 198.
[58] E. K. L. Yeow, A. H. A. Clayton, *Biophys. J.* **2007**, *92*, 3098 – 3104.
[59] M. H. Ulbrich, E. Y. Isacoff, *Nat. Methods* **2007**, *4*, 319 – 321.
[60] F. Yang, L. G. Moss, G. N. Phillips Jr. , *Nat. Biotechnol.* **1996**, *14*, 1246 – 1251.
[61] K. A. Lidke, B. Rieger, D. S. Lidke, T. M. Jovin, *IEEE Trans. Image Proc.* **2005**, *14*, 1237.
[62] A. Pralle, P. Keller, E. Florin, K. Simons, J. K. H. Hörber, *J. Cell Biol.* **2000**, *148*, 997 – 1007.
[63] I. A. Prior, C. Muncke, R. G. Parton, J. F. Hancock, *J. Cell Biol.* **2003**, *160*, 165 – 170.
[64] T. S. van Zanten, A. Cambi, M. F. Garcia-Parajo, *Biochim. Biophys. Acta Biomembr.* **2010**, *1798*, 777 – 787.
[65] J. F. Hancock, I. A. Prior, *Methods* **2005**, *37*, 165 – 172.
[66] S. Chiantia, J. Ries, P. Schwille, *Biochim. Biophys. Acta Biomembr.* **2009**, *1788*, 225 – 233.
[67] C. Eggeling, C. Ringemann, R. Medda, G. Schwarzmann, K. Sandhoff, S. Polyakova, V. N. Belov, B. Hein, C. Von Middendorff, A. Schönle, S. W. Hell, *Nature* **2009**, *457*, 1159 – 1162.
[68] N. Van Belzen, P. J. Rijken, W. J. Hage, S. W. De Laat, A. J. Verkleij, J. Boonstra, *J. Cell. Physiol.* **1988**, *134*, 413 – 420.
[69] S. Saffarian, Y. Li, E. L. Elson, L. J. Pike, *Biophys. J.* **2007**, *93*, 1021 – 1031.
[70] P. Nagy, J. Claus, T. M. Jovin, D. J. Arndt-Jovin, *Proc. Natl. Acad. Sci. USA* **2010**, *107*, 16524 – 16529.

Received: September 28, 2010
Published online on December 22, 2010

